Generating Single Microwave Photons in a Circuit

Project Report for **ELE 456**

Submitted by:

Md Shafayat Hossain

Graduate student

Introduction:

To enable communication between distinct parts of quantum computers, we need quantum signals consisting of single photons[1] which classical source is unable to provide. Although the idea of single photon generation started with collecting the fluorescence of a single atom[2, 3, 4] and advanced later to triggered photon source[5, 6, 7, 8, 9, 10, 11] on demand by placing the emitters inside the microwave[12, 13, 14, 15, 16, 17, 18, 19] or optical cavity for efficient collections of photons, on-chip implementation remained a challenge. Houck et al.[20] proposed on-chip single photon source within circuit quantum electrodynamics (CQED) architecture[21] with microwave transmission line cavity enhancing the spontaneous emission of single superconducting qubit. That spontaneously emitted photon then acts as a flying qubit and transfer information on-chip.

To generate non-classical photon states in a cavity, the states are a superposition of n = 0 and n = 1 Fock states with controlled amplitude and phase. 'Fluorescence tomography' is performed on these states using square law detection to determine the probability of having a photon. In addition, homodyne measurements is performed to determine the two quadratures of the electric field which are controlled by the off-diagonal coherence between the n = 0 and n = 1 Fock states. In particular the paper shows that the mean electric field of the one-photon Fock state is zero. In this project, we have reproduced the measurement results using Markovian Master Equation simulations.

This report starts with the motivation behind this project and advanced to the experimental implementation using the CQED architecture in transmon regime. Later sections deal with the mathematical formulation of the problem covering the celebrated Jaynes Cummings Hamiltonian for the system and Lindblad Master Equation for solving the dynamics of the system. Then, we put forward the calculated results and offered some explanation for verification of the single photon source.

Motivation:

In this project, full characterization of the qubit is performed by just looking at the spontaneous emission at the output, directly observing a superconducting qubit at its Larmor frequency. This entails that a qubit state at arbitrary points on the Bloch sphere can be transferred onto a photon state, thus moving information from a stationary qubit to a "flying qubit", one of the DiVincenzo resources for quantum information processing[22]. The mapping of qubit states onto photon states allows for the use of microwave photons as a true resource for quantum information on a chip. This is a convenient means of creating non-classical states of light to interact with atoms, in which the photon can be guided along the wires of an integrated circuit, allowing them to be shuttled around a chip. The generation of single photons, and superpositions of photon states, is an

important step towards on-chip quantum optics experiments and an important addition to toolbox for quantum optical experiments.

Moreover, this project deals with the Jaynes Cummings Hamiltonian, Master Equation for obtaining time dynamics of the system, Purcell physics and spontaneous emission problem in a driven dissipative regime for transmon qubit within CQED architecture which are covered in the course lectures and this project thus offers a platform for testing the knowledge obtained in the course.

Theory:

Principle of Single Photon Source:

When an atom or qubit is strongly coupled to a cavity, the spontaneous emission rate to the output mode of the cavity is enhanced. This process is known as the Purcell Effect[23] which is used here for triggering the single photon source[14, 15, 16]. Each time the qubit is excited with the control pulse, it can emit one and only one photon when it decays. When the qubit is put in an arbitrary superposition state, this state is mapped onto a superposition of zero and one photon, thus transferring information from a stationary to a flying qubit. Thus, the qubit can be an efficient photon source if this enhanced emission dominates over other relaxation channels $\gamma_\kappa \gg \gamma_{NR}$. This spontaneous emission rate can be determined from the Hamiltonian of the system, the well-known Jaynes–Cummings Hamiltonian

$$H = \frac{\hbar\omega_a\sigma_z}{2} + \hbar\omega_c\left(a^\dagger a + \frac{1}{2}\right) + \hbar g(a^\dagger\sigma_- + a\sigma_+) \quad (1)$$

Here the first term represents qubit with frequency ω_a described by Pauli operators σ_x, σ_y and σ_z, and raising, lowering operators σ_+ and σ_-

The second term represents a single cavity mode of frequency ω_c described by the photon creation and annihilation operators $a^\dagger$ and a

The final term represents a coupling of strength g between the qubit and the photon, which mixes the individual qubit and photon Eigen states

When far detuned ($\Delta = \omega_c - \omega_a \gg g$), the qubit acquires a small photonic component of the wave function, of magnitude g/Δ opening up a new source of decay for the qubit, as the photonic component of the qubit can emit at the cavity decay rate κ, resulting in a new qubit decay rate $\gamma_\kappa = (g/\Delta)^2\kappa$

Furthermore, when cavity and qubit are resonant, transmission measurement reveals two peaks instead of one for the detuned cavity-qubit system which is known as Vacuum Rabi splitting. Each peak corresponds to one of the two single-excitation eigenstates of the system, which are superpositions of the separate qubit and photon excitation states. The width of each peak is the average of the qubit and photon decay rates, (γ+κ)/2.
In the dispersive limit ($\Delta \gg g$), spontaneous emission is enhanced due to Purcell Effect resulting in approximate decay rates of $[1 - (g/\Delta)^2]\,\kappa + (g/\Delta)^2\,\gamma$ of the cavity and $[1 - (g/\Delta)^2]\gamma + (g/\Delta)^2\kappa$ of the qubit. Thus we can manipulate the rate of radiative decay of the qubit by tuning its frequency.

It is this enhanced qubit decay due to the cavity that is used in generating single photons: the qubit line broadens when the decay of the photon-like part of the wavefunction dominates the non-radiative qubit decay. The system parameters for the single photon source are chosen in such a way that these conditions satisfy.

Verification for single photon source:
Verifying the single photon output is a substantial challenge in on-chip microwave experiments. At the time of the experiment, microwave single photon detectors were in their infancy[1] and there isn't yet an equivalent to the optical single photon detector such as a photomultiplier or avalanche photodiode. However, several unique characteristics of the source are evident in the average signal generated by many single photon events, together yielding a convincing verification even with noisy detectors.

The expectation from the single photon source:

- Output of the single photon source is expected to be oscillatory in the amplitude of the control pulse.
- The average amplitude produced should agree well with the expected value for a single photon.
- Finally, and most importantly, if the output of the system depends only on the state of the qubit, the measured photons should show complete agreement with that expected from independent measurements of the qubit.

The source reported in Houck et al.[20] meets all three of these criteria.

In our calculation, we have used the following criteria for verification for single photon source:

- If the qubit state is mapped to the photon state, then an arbitrary superposition of the ground and excited states $\alpha|g\rangle + \beta|e\rangle$ will result in the same superposition of photon states: $\alpha|0\rangle + \beta|1\rangle$**,** where $|0\rangle$ and $|1\rangle$ refer to states with zero or one photon

- The average photon number *(<$a^\dagger a$>)* is proportional to the average qubit excitation probability *(<σ_z>)*, and has a maximum of one photon when the qubit is in the purely excited state.
- The two quadratures of homodyne voltage *[<$a^\dagger + a$>, i<$a^\dagger - a$>]* should be proportional to the x and y components of the qubit state *[<σ_x>,<σ_y>]*

System Implementation:

The challenge in implementing a single photon source (Figure 1) is to create a system where spontaneous emission dominates other relaxation channels. The Purcell enhanced qubit decay due to the cavity is used in generating single photons (Figure 2). Also, the qubit line broadens when the decay of the photon-like part of the wavefunction dominates the non-radiative qubit decay. Here, $\omega_a/2\pi$= 4.68 GHz with coupling, $g/2\pi$= 107 MHz resulting in $(g/\Delta)^2$ =4% photonic nature in qubit wavefunction and henceforth a spontaneous emission rate of $\gamma_\kappa/2\pi$=1.9 MHz. The experimental observation of relaxation rate of $\gamma/2\pi$=1.8$\pm$0.1 MHz substantiate the dominance of spontaneous emission over other relaxation channels to the output transmission line.

The source is implemented in a circuit quantum electrodynamics system consisting of a superconducting transmon qubit[24], an optimized version of the 'Cooper pair box[25], capacitively coupled to a half-wave transmission line cavity with fundamental frequency $\omega_c/2\pi$ = 5.19 GHz (Figure 1). Two important design differences between this circuit and previous incarnations of circuit quantum electrodynamics[1, 26] are needed to achieve efficient single-photon generation. First, the cavity is asymmetric in that the capacitors (mirrors) at either end of the transmission line are no longer identical, resulting in asymmetric decay rates to the input and output ports ($\kappa_{in}/2\pi$ ~ 200 kHz for the input side and $\kappa_{out}/2\pi$ = 44 MHz for the output). As a result, photons generated in the cavity are emitted at the output port more than 99% of the time. In addition, the total decay rate for the cavity, $\kappa/2\pi$ = 44 MHz, is substantially higher than in the samples made earlier for other experiments by the same group, a necessary change for spontaneous emission to be the dominant relaxation channel for the qubit.

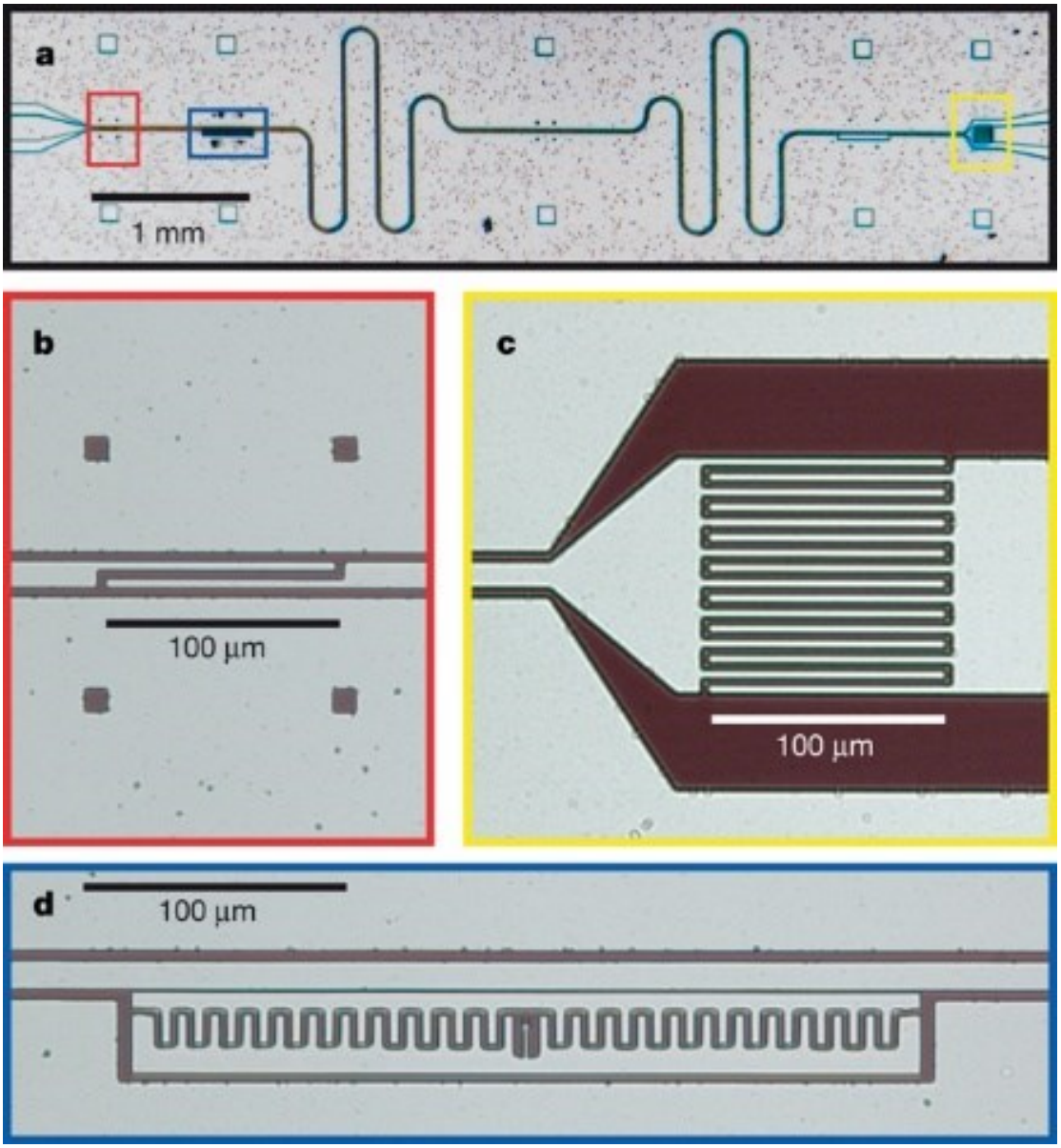

Figure 1: The circuit quantum electrodynamics device for generating single photons by Houck et al.[20]: **(a),** A transmission line cavity (180 nm Al on a SiO_2/Si substrate) is formed between two capacitors, with the input capacitor shown in **b** (red box in a) and the output in **c** (yellow box in a). Because the output capacitor is much larger, most radiation leaving the cavity leaves from this port, allowing efficient collection of light emitted from the cavity. **(d),** Transmon qubit (100-nm-thick aluminum), an optimized 'Cooper pair box', at a voltage anti-node of the cavity (blue box in **a**). The qubit is characterized by a Josephson energy, tuned by an applied magnetic field with a maximum of E_J^{max}/h = 20.2 GHz and a charging energy E_c/h = 0.37 GHz. The coupling to the cavity is $g/2\pi$ = 107 MHz at the qubit frequency primarily used in this paper, $\omega_a/2\pi$ = 4.68 GHz, and has a slight dependence on the qubit frequency. The transition from the first to second excited state, $\omega_{12}/2\pi$ = 4.19 GHz, is sufficiently different from ω_a to treat the qubit as a two-level system.

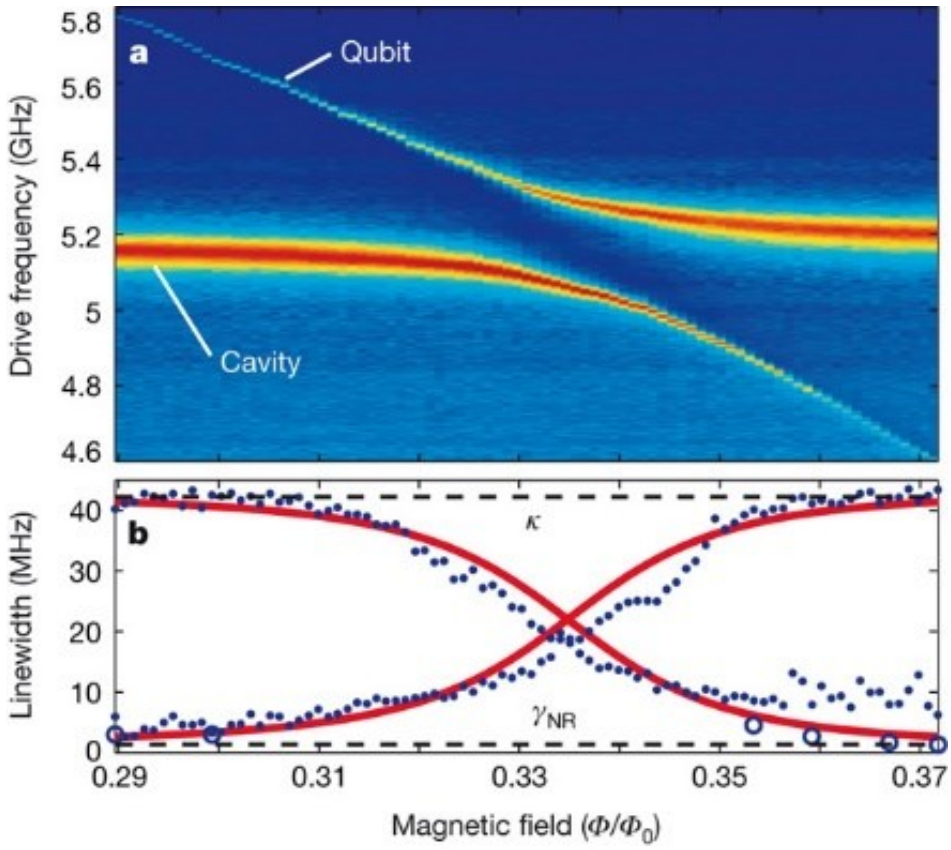

Figure 2: Experimental data for enhanced spontaneous emission through the Purcell effect**. a**) Transmission through the cavity–qubit system at different applied fluxes (log scale). Two peaks are evident in transmission due to the vacuum Rabi splitting. Away from the avoided crossing, these peaks correspond to 'mostly qubit' and 'mostly cavity' states. The bare linewidth of the cavity, $\kappa/2\pi$ = 44 MHz, is much larger than the bare qubit linewidth $\gamma_{NR}/2\pi$ < 2 MHz. **b**) Extracted linewidths from the data in **a** (blue dots) are compared with theoretical values (red lines). As the qubit and cavity peaks approach degeneracy, the qubit peak becomes broader owing to spontaneous emission to the cavity mode, while the cavity decay is suppressed. Extra dephasing present only at low frequencies (the right side of the graph) causes a non-lorentzian line shape and excessive width. Measurements of the relaxation rate in the time domain (open blue circles) agree with theoretical estimates. Discrepancies arise due to flux noise and variations in non-radiative decay with frequency. The operating point for the simulation carried out is Φ/Φ_0 = 0.366.

Mathematical Formulation of the Problem:

The Hamiltonian for the cavity-qubit system is the well-known Jaynes–Cummings Hamiltonian as in Eq. 1. Logical operations and readout of the qubit can be achieved by applying a microwave signal on the input port of the resonator. This can be modeled by the Hamiltonian:

$$H_d = \sum_k \hbar\left(\epsilon_k(t)a^\dagger e^{-i\omega_k t} + \epsilon_k^*(t)a e^{i\omega_k t}\right) \quad (2a)$$

Frequency that is close to the resonator frequency corresponds to a readout of the qubit's state and frequencies that are close to ω_a can be used to control the qubit. Here we are only interested in resonant drive. Thus our drive Hamiltonian for the control pulse is:

$$H_d = \hbar\left(\epsilon(t)a^{\dagger}e^{-i\omega_a t} + \epsilon^{*}(t)ae^{i\omega_a t}\right) \quad (2b)$$

Calibration of the Drive:

Integration of the pulse in time domain should be the Rabi angle. Area Normalized Gaussian pulse chosen. Then amplitude of the drive should be the Rabi angle. Practically the drive voltage is calibrated from observing the qubit state. For our simulation purpose, we can approximate it by using a hand-waving value of voltage for π pulse

$$V = \hbar \times \frac{qubit\ transition\ frequency}{electron\ charge} \quad (3)$$

And then we can apply some minor correction to match the experimental value.

Lindblad Master Equation:

For non-unitary evolution of a quantum systems, i.e., evolution that includes incoherent processes such as relaxation and dephasing, it is common to use master equations. While the evolution of the state vector in a closed quantum system is deterministic, open quantum systems are stochastic in nature. The effect of an environment on the system of interest is to induce stochastic transitions between energy levels, and to introduce uncertainty in the phase difference between states of the system. The state of an open quantum system is therefore described in terms of ensemble averaged states using the density matrix formalism. A density matrix ϱ describes a probability distribution of quantum states $|\psi_n\rangle$, in a matrix representation $\varrho = \sum_n P_n |\psi_n\rangle\langle\psi_n|$, where p_n is the classical probability that the system is in the quantum state $|\psi_n\rangle$.

We can apply following approximations to obtain the Master equation for our system.

1. **Separability:** At t=0 there are no correlations between the system and its environment such that the total density matrix can be written as a tensor product

$$\varrho_{tot}^{I}(0) = \varrho^{I}(0) \otimes \varrho_{env}^{I}(0) \quad (4)$$

2. **Born approximation:** It Requires:

a. that the state of the environment does not significantly change as a result of the interaction with the system

b. The system and the environment remain separable throughout the evolution.

These assumptions are justified if the interaction is weak, and if the environment is much larger than the system. In summary

$$\varrho_{tot}(t) \approx \varrho(t) \otimes \varrho_{env} \tag{5}$$

3. **Markov approximation:** The time-scale of decay for the environment τ_{env} is much shorter than the smallest time-scale of the system dynamics $\tau_{sys} \gg \tau_{env}$. This approximation is often deemed a "short-memory environment" as it requires that environmental correlation functions decay on a time-scale fast compared to those of the system.

4. **Secular approximation:** Elements in the master equation corresponding to transition frequencies satisfy $|\omega_{ab}-\omega_{cd}| \ll 1/\tau_{sys}$, i.e., all fast rotating terms in the interaction picture can be neglected.

After applying the approximations to the Liouville equation of motion ($\dot{\chi} = -\frac{i}{\hbar}\left[H, \chi\right]$), we get the Master equation

$$\dot{\varrho} = -\frac{i}{\hbar}\left[H, \varrho\right] + \kappa\mathcal{D}[a]\varrho + \gamma_1\mathcal{D}[\sigma_-]\varrho + \frac{\gamma_\varphi}{2}\mathcal{D}[\sigma_z]\varrho \tag{6}$$

$$H = H_s + H_d \tag{7}$$

$$\mathcal{D}[L]\varrho = \frac{2L\varrho L^\dagger - L^\dagger L\varrho - \varrho L^\dagger L}{2} \tag{8}$$

κ is the resonator rate of photon loss
γ_1 is the qubit energy decay rate
γ_φ is the qubit rate of pure dephasing

Moreover, the derivation of Eq. 6 is discussed in the class.

Dispersive Jaynes Cummings Hamiltonian:
In the limit where $|\Delta| \equiv |\omega_a - \omega_c| \gg g$, the Jaynes-Cummings Hamiltonian (Eq. 1) can be approximately diagonalized using the unitary transformation, $D_{Linear}=e^{\lambda I_-}$, (Here, $I_-=a^\dagger\sigma_- \pm a\sigma_+$) with $\lambda=g/\Delta$ a small parameter. Using the relation

$$e^{-\lambda X} H e^{\lambda X} = H + \lambda[H,X] + \frac{\lambda 2}{2!}[[H,X],X] + \cdots \quad (9)$$

To second order in λ, it is simple to obtain the effective Hamiltonian describing the dispersive regime,

$$Heff = D^{\dagger}_{Linear} H_s D_{Linear} = \hbar\omega_c a^{\dagger}a + \hbar\left(\omega_a + 2g\lambda\left[a^{\dagger}a + \frac{1}{2}\right]\right)\frac{\sigma_z}{2} + O(\lambda^2) \quad (10)$$

The qubit transition frequency is shifted by a quantity proportional to the photon population $2g\lambda\langle a^{\dagger}a\rangle$. Alternatively, this shift can be seen as a qubit-dependent pull of the resonator frequency $\omega_c \rightarrow \omega_c \pm g\lambda$.

As a result, shinning microwaves at the input port of the resonator at a frequency close to ω_c and measuring the transmitted signal using standard homodyne techniques serves as measurement of the qubit. In this approximation, this corresponds to a quantum nondemolition (QND) measurement of the qubit. For our system, we will assume that, it operates in linear regime.

Qubit Relaxation and Photon Decay:

Energy damping of the resonator (κ) and of the qubit (γ_1) can be modeled by coupling to baths of harmonic oscillators with free Hamiltonians

$$H_{B\kappa} = \hbar \int_0^{\infty} \omega b_k^{\dagger}(\omega) b_k(\omega) d\omega \quad (11)$$

$$H_{B\gamma} = \hbar \int_0^{\infty} \omega b_{\gamma}^{\dagger}(\omega) b_{\gamma}(\omega) d\omega \quad (12)$$

$b_{k,\gamma}^{\dagger}(\omega)$, $b_{k,\gamma}(\omega)$ are creation and annihilation operator in the qubit bath.

Coupling to these baths is described by:

$$H\kappa = i\hbar \int_0^{\infty} \sqrt{d_{\kappa}(\omega)}\,[f_{\kappa}^{*}(\omega) b_{\kappa}^{\dagger}(\omega) - H.c.](a + a^{\dagger}) d\omega \quad (13)$$

$$\mathrm{H}\gamma = i\hbar \int_0^{\infty} \sqrt{d_{\gamma}(\omega)}\,[f_{\gamma}^{*}(\omega) b_{\gamma}^{\dagger}(\omega) - H.c.]\sigma_{\mathrm{x}}\mathrm{d}\omega \quad (14)$$

Where $d_i(\omega)$ is the density of modes of bath i and $f_i(\omega)$ represents the coupling strength of the mode of frequency ω to the resonator or the qubit. Dephasing in the bare basis occurs due to slow fluctuations of the qubit transition frequency. Dephasing can be modeled by adding the Hamiltonian

$$H_{\varphi} = \hbar\nu f_{\varphi}(t)\sigma_z \quad (15)$$

In this expression, $f_\phi(t)$ is a random function of time with zero mean and v is characteristic of the magnitude of the coupling of the qubit to the fluctuations. Defining

$$f_\varphi(t) = \int_{-\infty}^{\infty} f_\varphi(\omega) e^{i\omega t} d\omega \tag{16}$$

H_ϕ can be written in frequency space as

$$H_\varphi = \hbar v \sigma_z \int_{-\infty}^{\infty} f_\varphi(\omega) e^{i\omega t} d\omega \tag{17}$$

Dispersive Master Equation:

Applying the dispersive transformation on the Hamiltonian, moving to the interaction frame by transformation of $e^{[-i(H_s + H_{B\kappa} + H_{B\gamma})t/\hbar]}$ and performing a rotating wave approximation yields

$$H_\kappa^D = i\hbar[L_1 z_\kappa^\dagger(t, \omega_c) + L_2 z_\kappa^\dagger(t, \omega_a)] + H.c. \tag{18}$$

$$H_\gamma^D = i\hbar[L_3 z_\gamma^\dagger(t, \omega_a) + L_4 z_\gamma^\dagger(t, \omega_c)] + H.c. \tag{19}$$

$$with\ L_1 = a(1 + \lambda^2\sigma_z/2), \qquad L_2 = \lambda\sigma_-, L_3 = \sigma_-[1 - \lambda^2(a^\dagger a + 1/2)], and\ L_4 = \lambda a\sigma_z.$$

The bath operators $z_i(t,\omega_p)$ are given by

$$z_i(t, \omega_p) = \int_{\omega_p - B_i, p}^{\omega_p + B_i, p} \sqrt{d_i(\omega)} f_i(\omega) b_i(\omega) e^{-i(\omega - \omega_p)t} d\omega \tag{20}$$

We have kept in Eq. 18 and 19 only terms that will contribute up to order λ^2 in the master equation. In obtaining this expression, we have taken the (dispersive) system Hamiltonian as $H_s \approx \hbar\omega_c a^\dagger a + \hbar\omega_a \sigma_z/2$, where ω_a is understood as the Lamb and ac-Stark shifted qubit transition frequency and ω_c is understood as the cavity frequency shifted by the nonlinearity (i.e., $\omega_c + \zeta$). Moreover, to perform the RWA, we have made the standard assumption that the system-bath interaction is limited to a small band of frequency $B_{i,p}$ around the frequency ω_p of the corresponding system operator L_i, $B_{i,p} \ll \omega_p$.

We now assume that, within the bandwidths $B_{i,p}$, the coupling constants $f_i(\omega_p)$ and the density of modes $d_i(\omega)$ do not vary significantly. In this situation, the above system-bath Hamiltonians can be rewritten as

$$H_\kappa^D = i\hbar\sqrt{\kappa_c} L_1 b_{\kappa,c}^\dagger(t) + i\hbar\sqrt{\kappa_a} L_2 b_{\kappa,a}^\dagger(t) + H.c. \tag{21}$$

$$H_\gamma^D = i\hbar\sqrt{\gamma_a}L_3 b_{\gamma,a}^\dagger(t) + i\hbar\sqrt{\gamma_c}L_4 b_{\gamma,c}^\dagger(t) + H.c. \tag{22}$$

Here, the decay rates are given by:

$$\kappa_p = 2\pi d_k(\omega_p)\left|f_\kappa(\omega_p)\right|^2 \tag{23a}$$

$$\gamma_p = 2\pi d_\gamma(\omega_p)\left|f_\gamma(\omega_p)\right|^2 \tag{23b}$$

$$\gamma_\varphi = 2\nu^2 S \tag{23c}$$

$$\gamma_{\pm\Delta} = 4\lambda^2\nu^2 S\,(\pm\Delta) \tag{23d}$$

Bath temporal modes are defined by:

$$b_{i,p}(t) = \frac{1}{\sqrt{2\pi}}\int_{\omega_p - B_i,p}^{\omega_p + B_i,p} d\omega b_i(\omega) e^{-i(\omega-\omega_p)t} \tag{24}$$

Since $[b_i(\omega), b^\dagger_j(\omega')] = \delta_{i,j}\delta(\omega-\omega')$, the commutator of two temporal modes is (after a change of integration variable)

$$[b_{i,p}(t), b_{j,q}^\dagger(t')] = \frac{\delta_{i,j}}{2\pi}\int_{-B_i,p}^{B_i,p}\int_{-B_i,q}^{B_i,q} d\omega d\omega' \delta(\omega - \omega' - \omega_p + \omega_q) e^{-i\omega t} e^{-i\omega' t'} \tag{25}$$

If we now take $|\omega_p - \omega_q| \gg B_{i,p}, B_{i,q}$ for $p \neq q$, then the above becomes

$$[b_{i,p}(t), b_{j,q}^\dagger(t')] = \frac{\delta_{i,j}\delta_{p,q}}{2\pi}\int_{-B_i,p}^{B_i,p} d\omega e^{-i\omega(t-t')} \tag{26}$$

In other words, we assume the bath operators to be independent. In the dispersive regime, this is a reasonable assumption since $|\omega_p - \omega_q| \sim \Delta$, where the detuning $|\Delta| \gg g$ is large.
We finally make the standard and reasonable assumption that dissipation is not too strong, such that the time scales set by the decay rates κ_p and γ_p are much longer than the cutoff time $1/B_{i,p}$. In this situation, we can effectively take the limit $B_{i,p} \to \infty$. This corresponds to the standard Markov approximation, which was already successfully applied to describe circuit QED experiments. In this situation, the above commutation relation reduces to

$$[b_{i,p}(t), b_{j,q}^\dagger(t')] = \delta_{i,j}\delta_{p,q}\delta(t-t') \tag{27}$$

In this Markov, or white noise, approximation the evolution operators can be written in Itô form as

$$U(t+dt,t) = U_\kappa(t+dt,t)U_\gamma(t+dt,t)e^{-iH_{tot}dt} \tag{28}$$

With

$$U_\kappa(t+dt,t) = exp\{-i\sqrt{\kappa_c}[L_1 dB^\dagger_{\kappa,c} - L_1^\dagger dB_{\kappa,c}] - i\sqrt{\kappa_a}[L_2 dB^\dagger_{\kappa,a} - L_2^\dagger dB_{\kappa,a}]\}U_\kappa(t) \tag{29}$$

$$U_\gamma(t+dt,t) = exp\{-i\sqrt{\gamma_a}[L_3 dB^\dagger_{\gamma,a} - L_3^\dagger dB_{\gamma,a}] - i\sqrt{\kappa_a}[L_4 dB^\dagger_{\gamma,c} - L_4^\dagger dB_{\gamma,c}]\}U_\gamma(t) \tag{30}$$

Where $dB_{i,p}=b_{i,p}dt$ is a quantum Wiener increment.

We now take the bath to be in the vacuum state and uncorrelated to the system at time t=0. By tracing over the bath and keeping terms of order O(dt) using Itô calculus, we obtain a Lindblad form master equation for the resonator-qubit system. In this master equation, the photon bath κ leads to the damping superoperators

$$\kappa\mathcal{D}\left[a\left(1+\frac{\lambda^2\sigma_z}{2}\right)\right]\varrho^D + \gamma_\kappa D[\sigma_-]\varrho^D \tag{31}$$

While the qubit bath γ leads to

$$\gamma\mathcal{D}\left[\sigma_-\left\{1-\lambda^2\left(a^\dagger a+\frac{1}{2}\right)\right\}\right]\varrho^D + \kappa\gamma D[a\sigma_z]\varrho^D \tag{32}$$

Thus we obtain the final equation:

$$\begin{aligned}\dot{\varrho}^D &= -\frac{i}{\hbar}\left[H_s^D + H_d^D,\ \varrho^D\right] + \kappa\mathcal{D}\left[a\left(1+\frac{\lambda^2\sigma_z}{2}\right)\right]\varrho^D \\ &\quad + \gamma_\kappa\mathcal{D}[\sigma_-]\varrho^D + \gamma\mathcal{D}\left[\sigma_-\left\{1-\lambda^2\left(a^\dagger a+\frac{1}{2}\right)\right\}\right]\varrho^D \\ &\quad + \kappa_\gamma\mathcal{D}[a\sigma_z]\varrho^D + \frac{\gamma_\varphi}{2}\mathcal{D}\left[\sigma_z\left\{1-2\lambda^2\left(a^\dagger a+\frac{1}{2}\right)\right\}\right]\varrho \\ &\quad + \gamma_\Delta\mathcal{D}[a^\dagger\sigma_-]\varrho^D + \gamma_{-\Delta}\mathcal{D}[a\sigma_+]\varrho^D \\ &= \mathcal{L}_D\varrho^D\end{aligned} \tag{33}$$

Where,

$$\lambda = \frac{g}{\Delta} \tag{34}$$

$$\kappa = \kappa_c, \gamma_\kappa = \lambda^2 \kappa_a, \gamma = \gamma_a, \kappa_\gamma = \lambda^2 \gamma_c \tag{35}$$

d is the density of modes

In order to ensure that the approximations behind the derivation of the Master equation are not violated, it is important that the decay rates γ_n be smaller than the minimum energy splitting in the system Hamiltonian which is valid in this case. The detailed derivation for dispersive master equation is done in Boissonneault et al.[27]

Results and Discussion:

1. Calibration of the drive

For a fixed width Gaussian pulse, Rabi angle (the angle at which the qubit is rotated) is proportions to control pulse amplitude (Figure 3). The control pulse amplitude is calibrated to equivalent Rabi angle by varying the drive amplitude and observing the qubit state rotation. Calibrated drive and corresponding spontaneous emission voltage are shown in Figure 4.

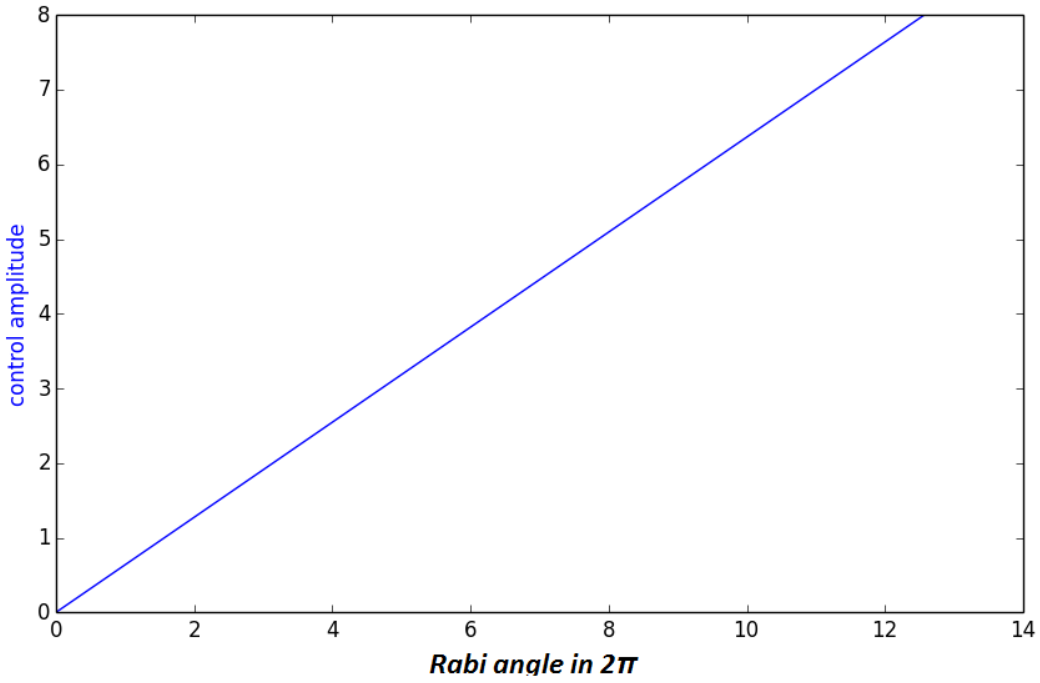

Figure 3: Calibration of the drive against Rabi angle (in units V_0 =2μV)

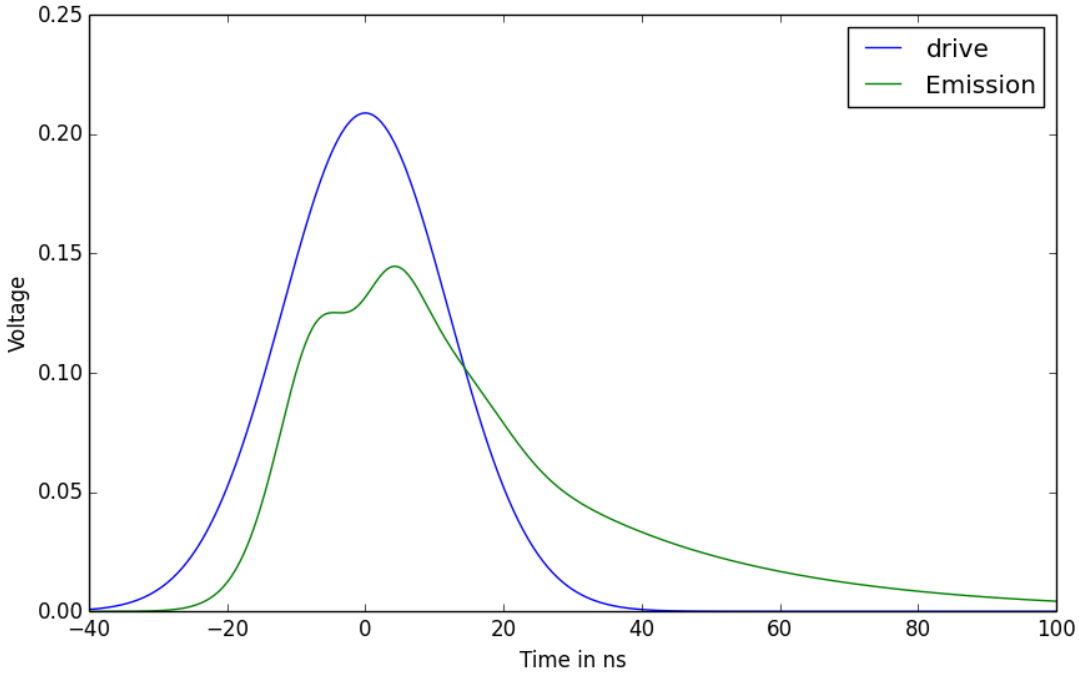

Figure 4: The time sequence, with a Gaussian pulse at the qubit frequency and subsequent photon emission with relaxation time T_1.

2. Mapping of qubit state onto photon states

The first step towards the verification of single photon source is to show that the output of the cavity is an oscillatory function of the input drive, as at most one photon is generated, regardless of the magnitude of the input drive.

A Gaussian pulse at qubit frequency with σ=12 ns rotates the qubit state by a Rabi angle that is proportional to the pulse amplitude. The excited qubit will then relax, generating a new photon state at the qubit frequency. Because the control pulse leaves the cavity at a rate that is much faster than the rate of spontaneous emission, γ_κ, the control pulse and the generated photons are temporally separable. As shown in the Figure 5a and 5b, while the spontaneous emission oscillates as the qubit is rotated from the ground to the excited state and back, confirming that the spontaneous emission is proportional to the qubit state, not simply to the applied drive amplitude. This is the key point of the scheme. We can conclude that, a superposition of many photons incoming on one temporal mode give rise to one (and only one) photon on a distinct outgoing temporal mode. Moreover, because a single photon is the maximum output, the source is insensitive (to first-order) to fluctuations in the control pulse when generating one photon.

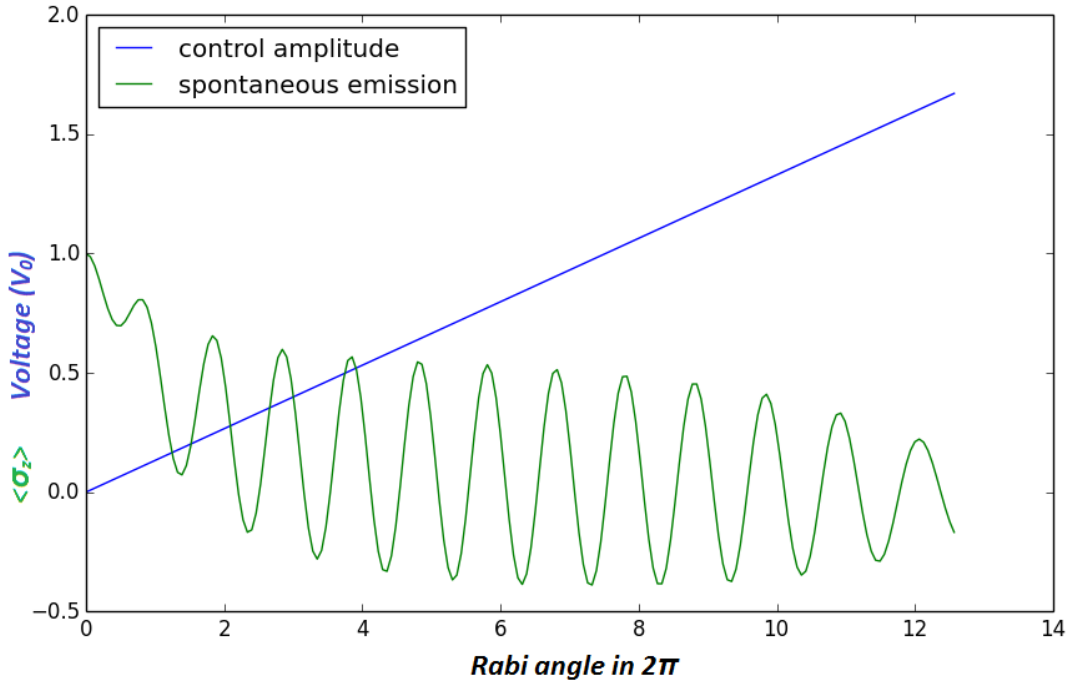
control amplitude
spontaneous emission
Voltage (V_0)
$\langle\sigma_z\rangle$
Rabi angle in 2π

(a)

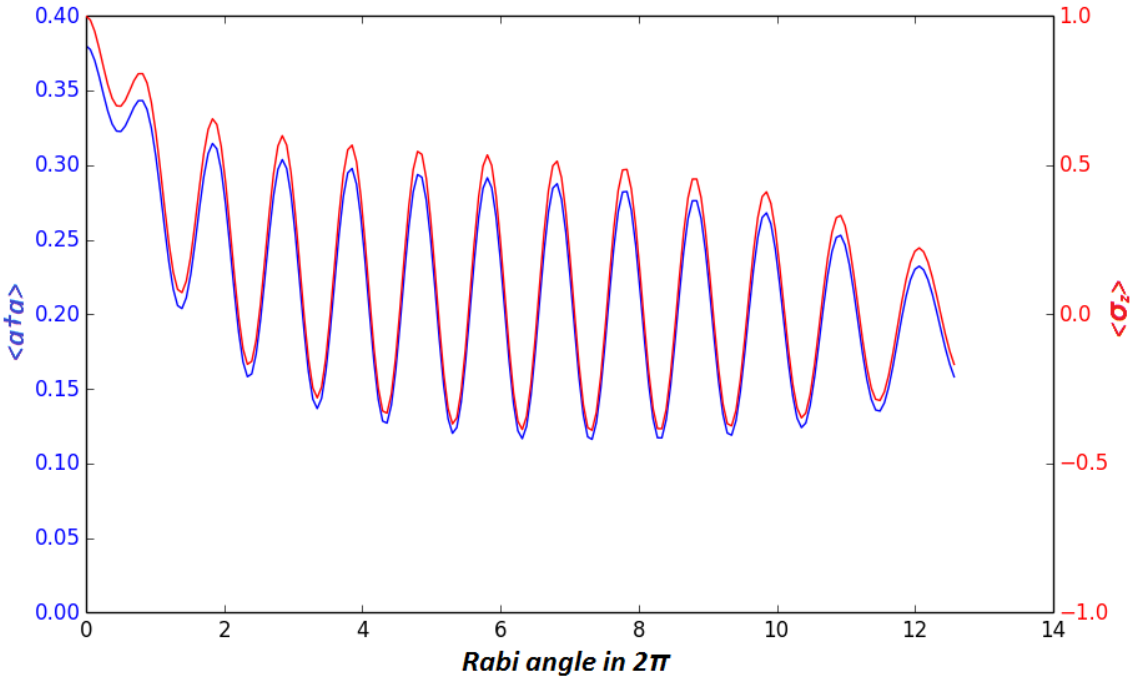
$\langle a^\dagger a\rangle$
$\langle\sigma_z\rangle$
Rabi angle in 2π

(b)

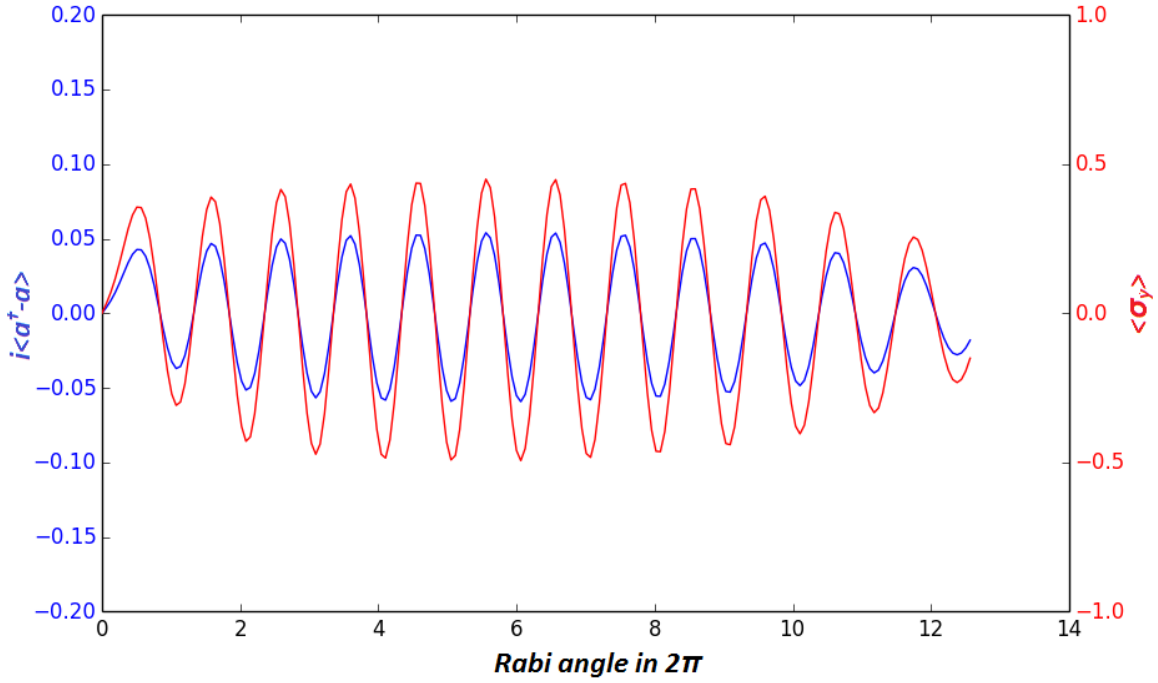

(c)

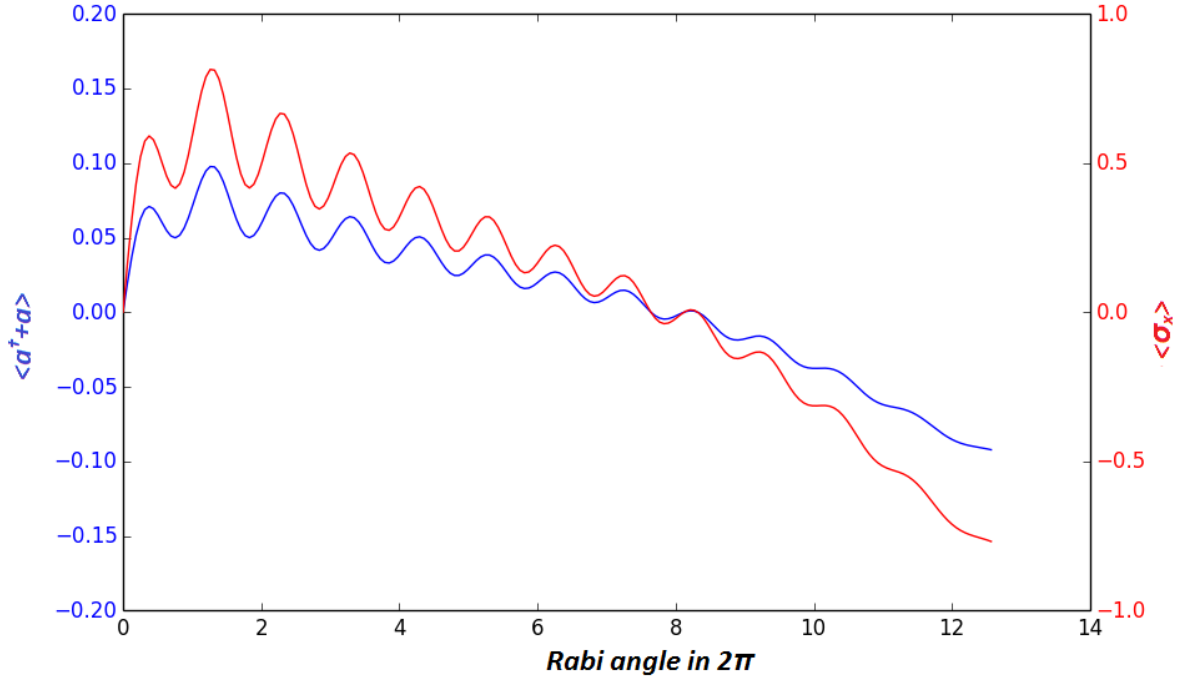

(d)

Figure 5: **a)** Simulated drive (in units of zero point fluctuation, V_0 =2μV) and spontaneous emission. When the drive rotating the qubit is increased, the initial output of the cavity increases

linearly, while after many lifetimes the output voltage of the cavity is oscillatory, due to photons stored in the qubit. **b)** Simulated photon number output of the cavity $< a^{\dagger}a >$ (calculated by integrating the photon number $<a^{\dagger}a>$ from t = 36 ns to t = 236 ns) and qubit state $\langle \sigma_z \rangle$ (calculated at steady state at t=36 ns). These peak when the qubit is in the excited state, after a π pulse; the agreement between qubit and photon states verifies the photon generation occurs as expected. In practical, because of measurement transients, spontaneous emission can be collected earlier after the drive than the qubit state can be measured. While the qubit and photon states do agree in amplitude at this time, the earlier emission is plotted in Houck et al. with a scaled version of the qubit state for signal to noise reasons. To match with the results in Houck et al., 38% collection efficiency of photon is considered. **c)** Integrated voltage of the output photons $i<a^{\dagger} - a>$ (integrated from t = 36 ns to t = 104 ns) compared with the qubit state $\langle \sigma_y \rangle$ calculated at steady state (in practice, it can be measured with a Ramsey experiment). **d)** Other quadrature of the homodyne voltage of the output photons $<a^{\dagger} + a>$ (integrated from t = 36 ns to t = 104 ns) compared with the qubit state $\langle \sigma_x \rangle$ calculated at steady state. The agreement between the quadrature of the homodyne voltages of the output photons and qubit states show that the phase of superposition states is also transferred from qubit to photon. Only 12% of the voltage for the π/2 superposition is collected in Houck et al., owing to non-radiative decay and qubit dephasing, setting the scale of the voltage axis. The qubit amplitude in the experiment is also extrapolated to the time immediately following the control pulse. To match with the experimental results, the 12% voltage collection efficiency is considered.

3. Simulating the free induction decay of a single qubit:

From the time dynamics obtained from the simulation of Master Equation, we can observe that the control and generated photons are orthogonal in phase allowing them to be separated in homodyne detection (Figure 6a and 6c). This is due to the fact that the control pulse sets the rotation axis, and the qubit state sets the orthogonal emission phase. In the generated photon quadrature (Figure 6g and 6h), rapid time oscillations are apparent during the control pulse; this is a direct observation of the Rabi oscillation of the qubit through its spontaneous emission. After the pulse, the qubit emits with a phase depending on its final state, thus results in oscillations in the control amplitude that smoothly connect to the temporal oscillations.

From the simulation, we can characterize the efficiency of the single photon source and define two metrics of efficiency: source efficiency and usable source efficiency.

The source efficiency is the fraction of time in which a photon is emitted after a control pulse. This depends on the final polarization of the qubit and the ratio of radiative to non-radiative channels. In generating a single photon, the π-pulse leaves the qubit 90% polarized (Figure 6d), and nearly all decay is radiative (γ_κ/γ>90%) giving source efficiency of more than 81% which is very close to the experimentally reported value of 78%

For generating a superposition of zero and one photon, the quadrature phase of the photon must also be controlled. Here, the qubit is 80% polarized along σ_y (Figure 6f), but a dephasing rate, γ_φ ~ 1 MHz leads to only $\gamma_\kappa/(\gamma+2\gamma_\varphi)$= 50% radiation efficiency, giving a total source efficiency of 40%.

A second metric, the usable source efficiency, is somewhat lower for this scheme, because the control pulse is slow and a delay is necessary to reject any control photons which could give a double-photon event. The collection of radiation begins after three standard deviations (36 ns) of the control pulse Gaussian, making the likelihood of contamination by a control photon less than 0.01%. Integrating the measured spontaneous emission, the number of detected photons is measured directly, yielding an efficiency of 38% for the single-photon source, and 12% for the homodyne voltage of the superposition state, which is again lower, owing to dephasing. Even after rejecting the emission contaminated by control pulse photons, which contains the high signal-to-noise part of the emission, a substantial fraction of one photon is recovered. However, this could be improved further with faster pulses, longer coherence times, or fast tunability of the qubit frequency, achieving usable source efficiencies close to 100%.

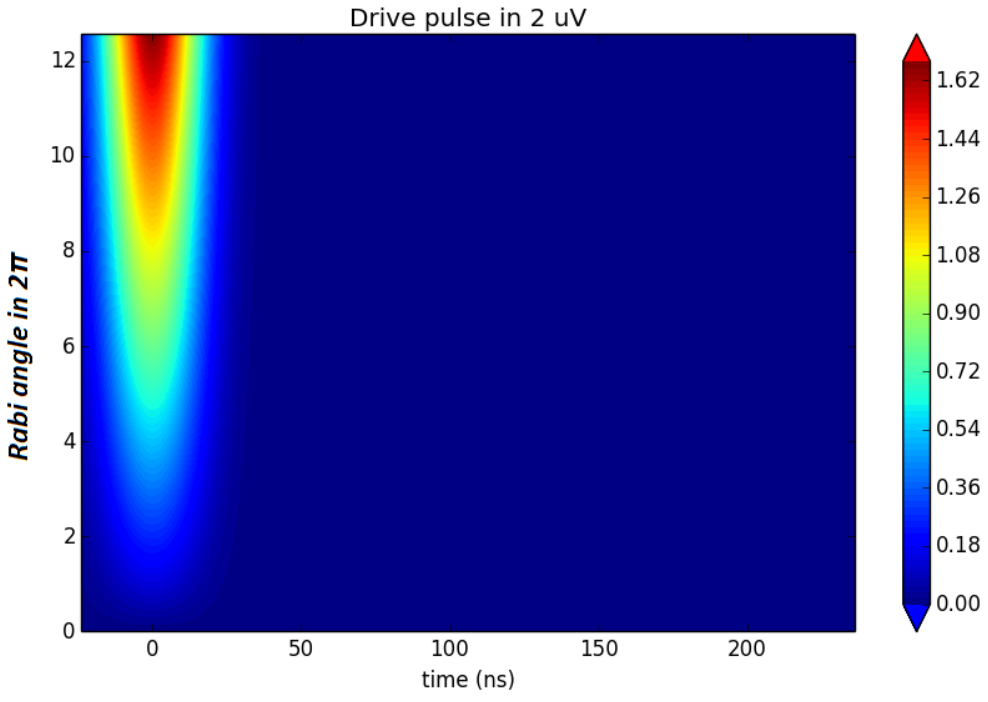

(a)

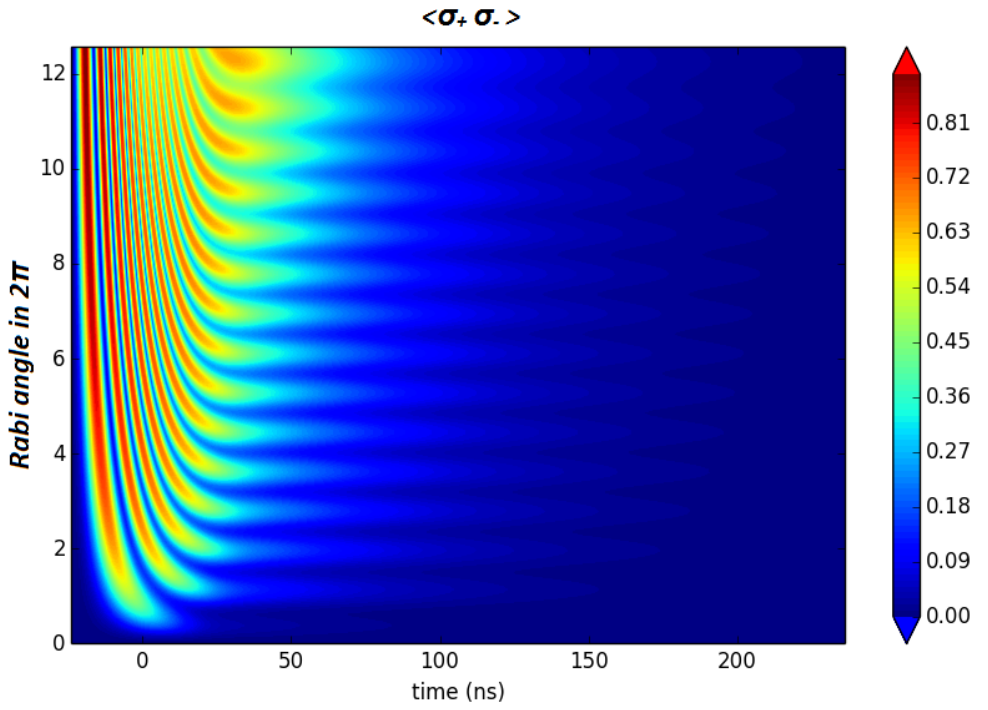
<σ+ σ- >
Rabi angle in 2π
time (ns)
0
2
4
6
8
10
12
0
50
100
150
200
0.81
0.72
0.63
0.54
0.45
0.36
0.27
0.18
0.09
0.00

(b)

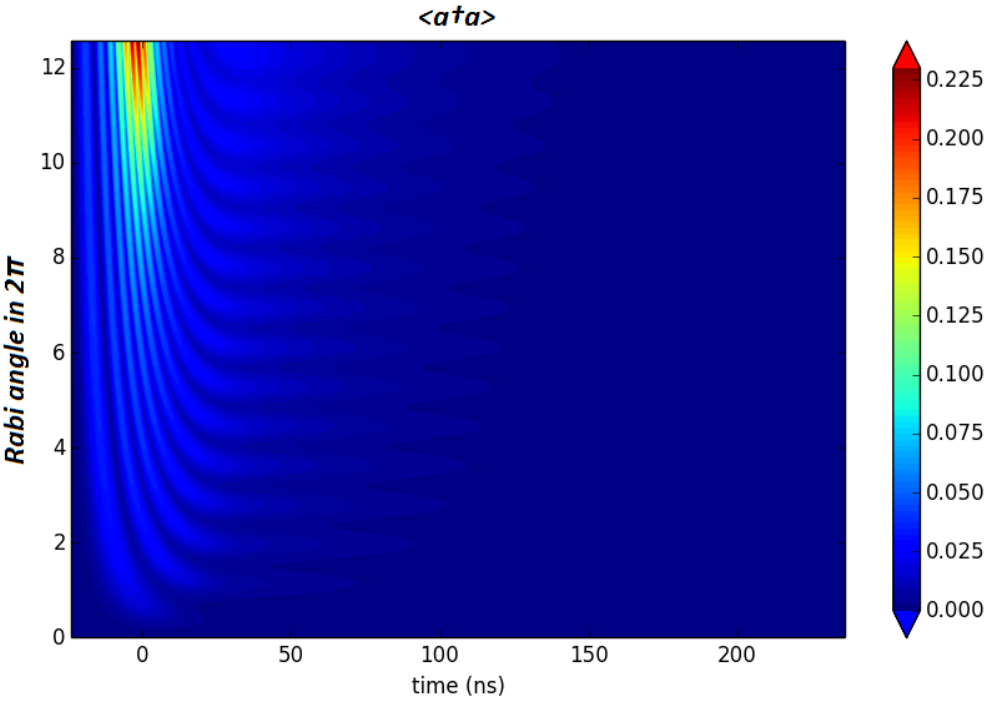
<a†a>
Rabi angle in 2π
time (ns)
0
2
4
6
8
10
12
0
50
100
150
200
0.225
0.200
0.175
0.150
0.125
0.100
0.075
0.050
0.025
0.000

(c)

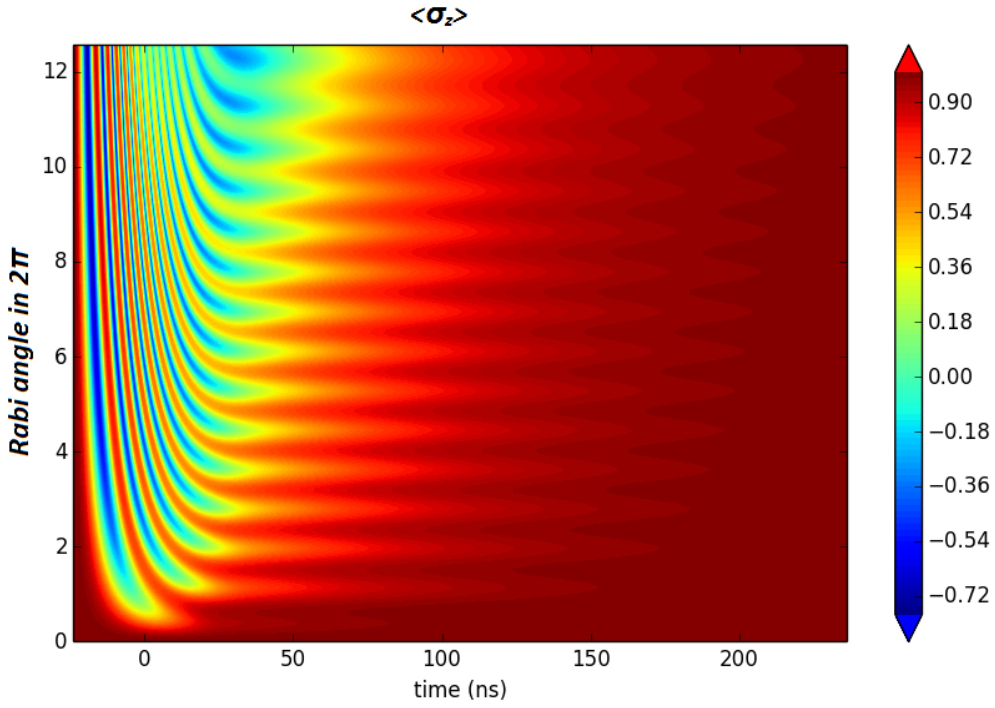
<σz>
Rabi angle in 2π
time (ns)
0
2
4
6
8
10
12
0
50
100
150
200
0.90
0.72
0.54
0.36
0.18
0.00
−0.18
−0.36
−0.54
−0.72

(d)

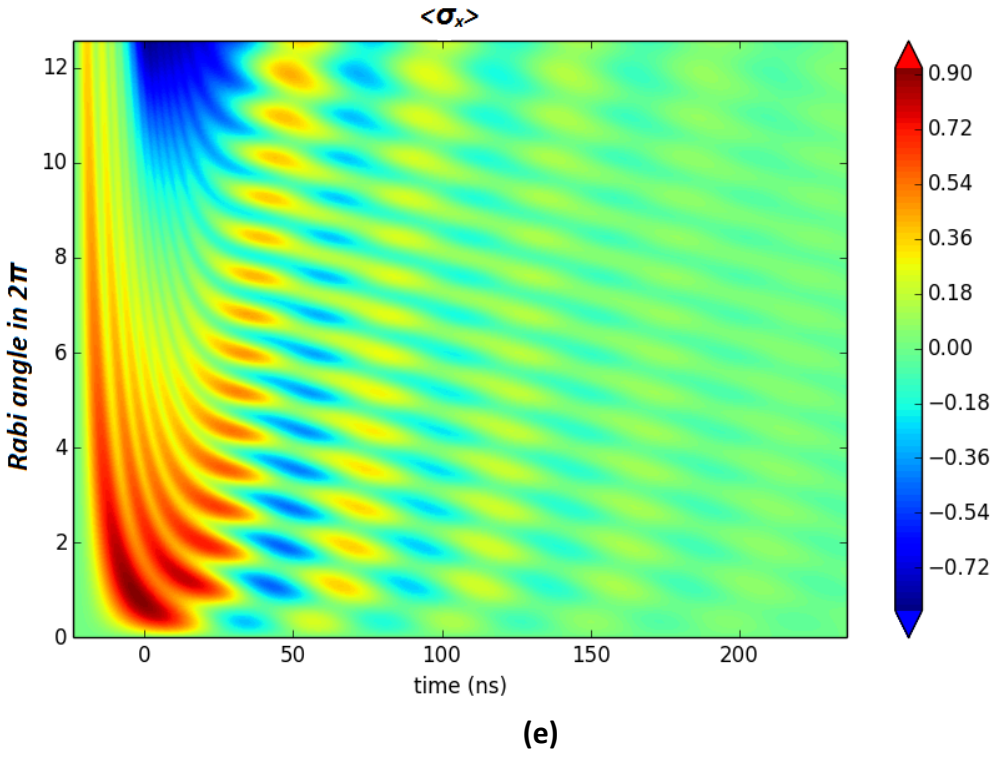
<σx>
Rabi angle in 2π
time (ns)
0
2
4
6
8
10
12
0
50
100
150
200
0.90
0.72
0.54
0.36
0.18
0.00
−0.18
−0.36
−0.54
−0.72

(e)

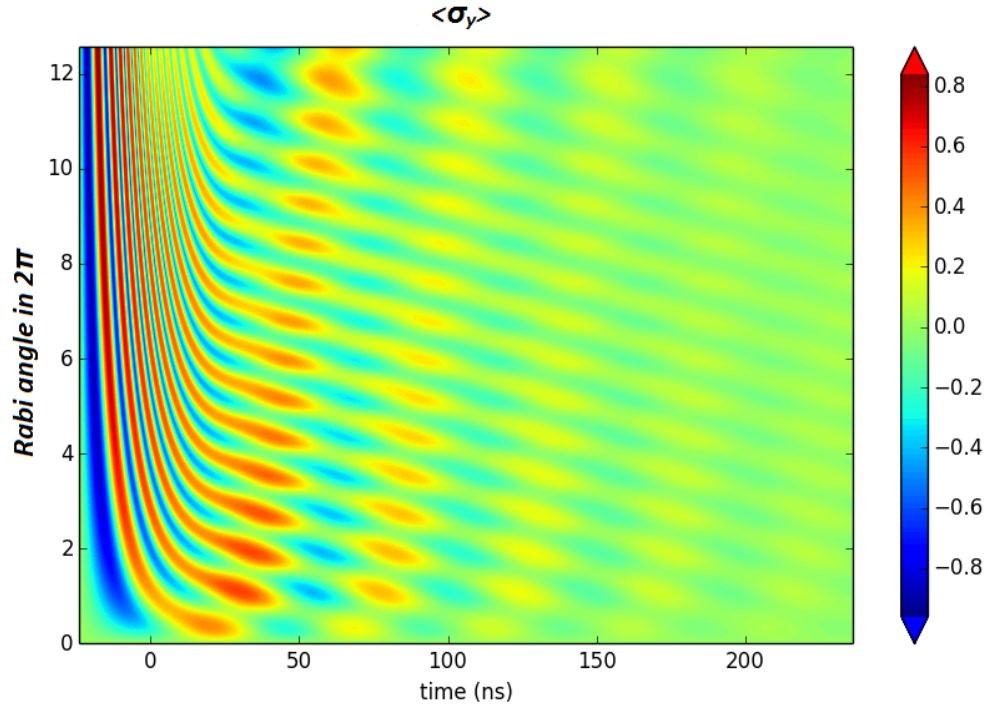
<σy>
Rabi angle in 2π
time (ns)
0
2
4
6
8
10
12
0
50
100
150
200
0.8
0.6
0.4
0.2
0.0
−0.2
−0.4
−0.6
−0.8

(f)

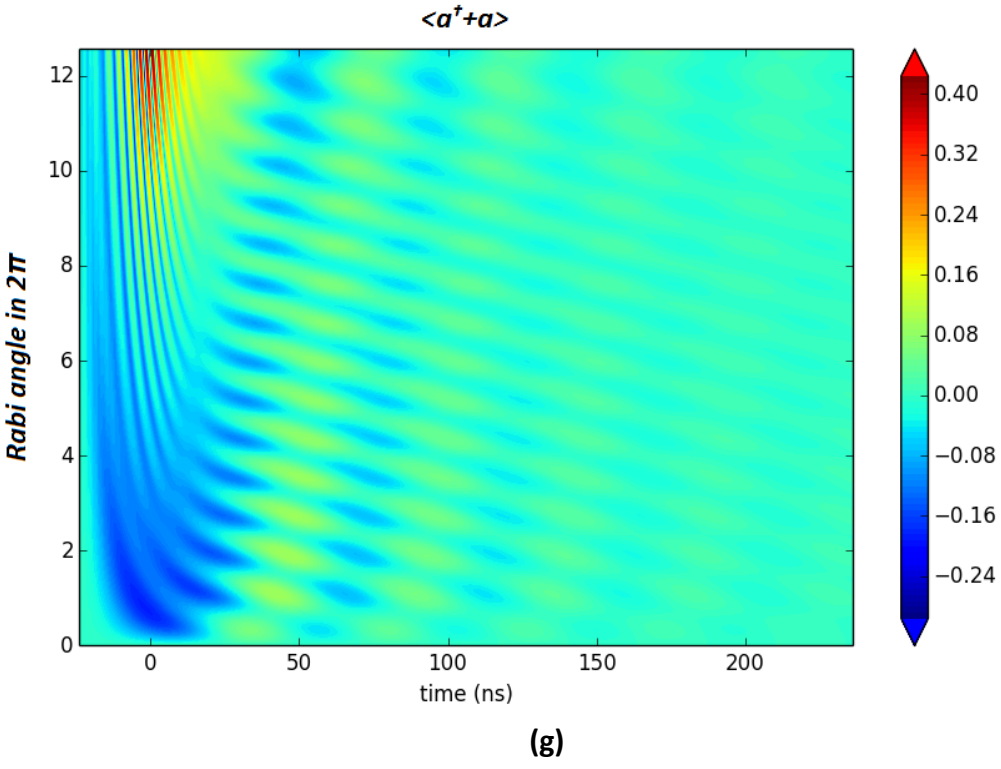
<a†+a>
Rabi angle in 2π
time (ns)
0
2
4
6
8
10
12
0
50
100
150
200
0.40
0.32
0.24
0.16
0.08
0.00
−0.08
−0.16
−0.24

(g)

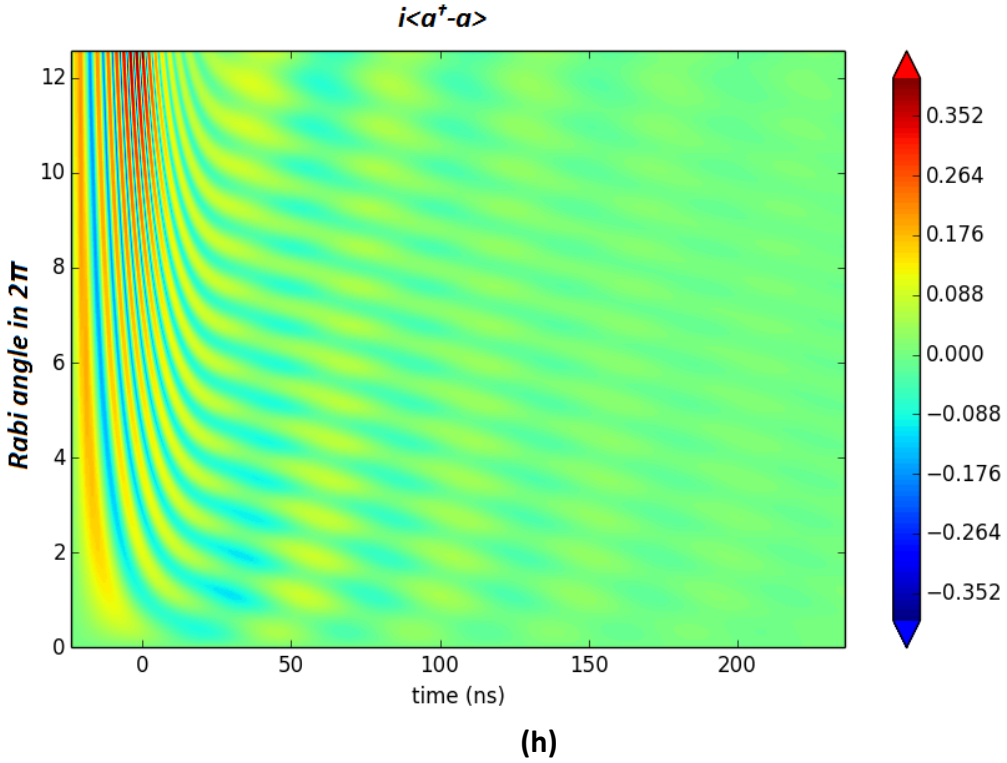

(h)

Figure 6: Measuring the free induction decay of a single qubit. **(a)**. Simulation for homodyne voltage in-phase with the drive. **(b)** and **(c)**. Decay in excitation probabilities of qubit ($\langle\sigma_+\sigma_-\rangle$) and cavity (< $a^\dagger a$ >) **(d), (e)** and **(f).** Qubit state $\langle\sigma_z\rangle$, $\langle\sigma_x\rangle$, $\langle\sigma_y\rangle$. **(g)** and **(h).** Both quadrature of the homodyne voltage (<$a + a^\dagger$> and i<$a^\dagger$- a>). Because emission is always orthogonal to the rotation axis, the spontaneous emission and control signal are phase separable. The homodyne sine waves in the previous figure are vertical slices through the emission. The frequency of these oscillations, coupled with a gain known from measurements of the control pulse, provide a calibration. The simulation presented here uses this calibration to predict the experimental data provided in Houck et al. The fast oscillations in the time domain are a direct measure of the Rabi oscillations of the qubit.

4. Fluorescence Tomography for the Single Photon Source

Tomography is a powerful tool for characterizing the interplay between qubit state[28] and photon state[29, 30]. Here, qubit tomography is performed by applying control pulses of arbitrary phase and amplitude, and performing a dispersive readout of the qubit states. This yields the expected concentric rings for a qubit state $\langle\sigma_z\rangle$ initially in the ground state (Figure 7a). Similarly, for the same set of control pulses, both quadrature (Figure 7b and 7d) of the output homodyne voltage are calculated. These show excellent agreement with $\langle\sigma_x\rangle$ (Figure 7c), $\langle\sigma_y\rangle$ (Figure 7e) components of the qubit state. Thus, this technique fully characterizes the transfer from qubit state to photon state.

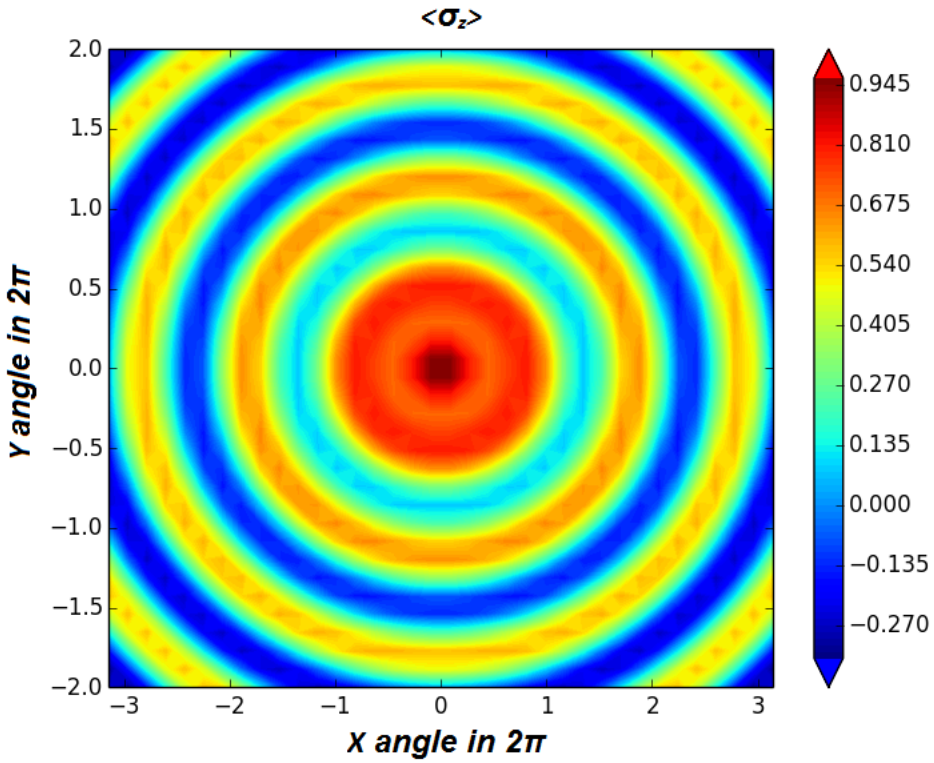
<σz>
2.0
1.5
1.0
0.5
0.0
−0.5
−1.0
−1.5
−2.0
Y angle in 2π
−3
−2
−1
0
1
2
3
X angle in 2π
0.945
0.810
0.675
0.540
0.405
0.270
0.135
0.000
−0.135
−0.270

(a)

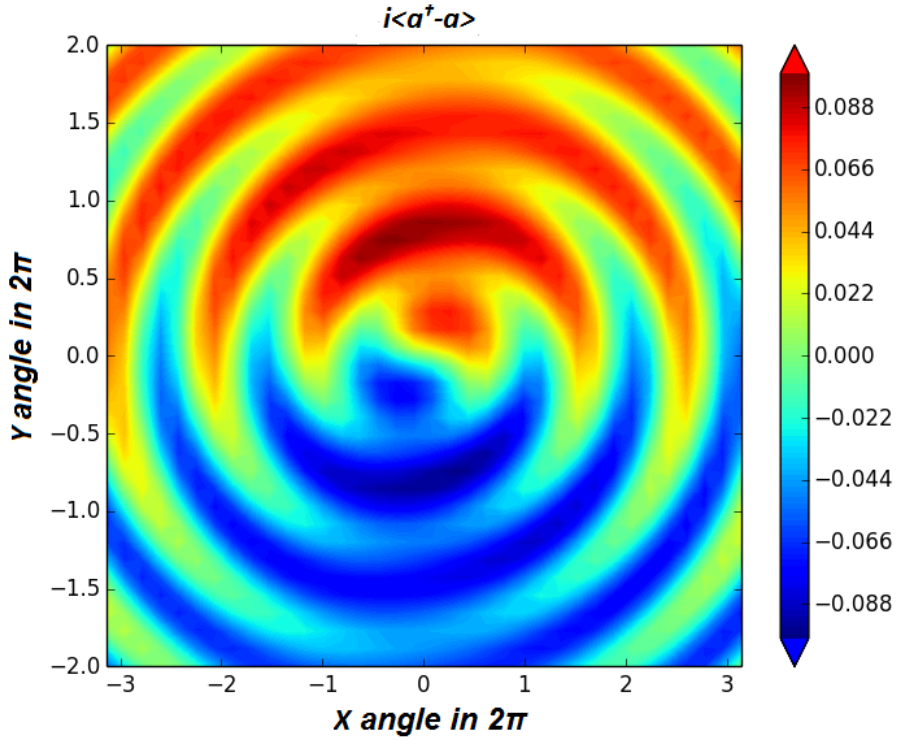
i<a†-a>
2.0
1.5
1.0
0.5
0.0
−0.5
−1.0
−1.5
−2.0
Y angle in 2π
−3
−2
−1
0
1
2
3
X angle in 2π
0.088
0.066
0.044
0.022
0.000
−0.022
−0.044
−0.066
−0.088

(b)

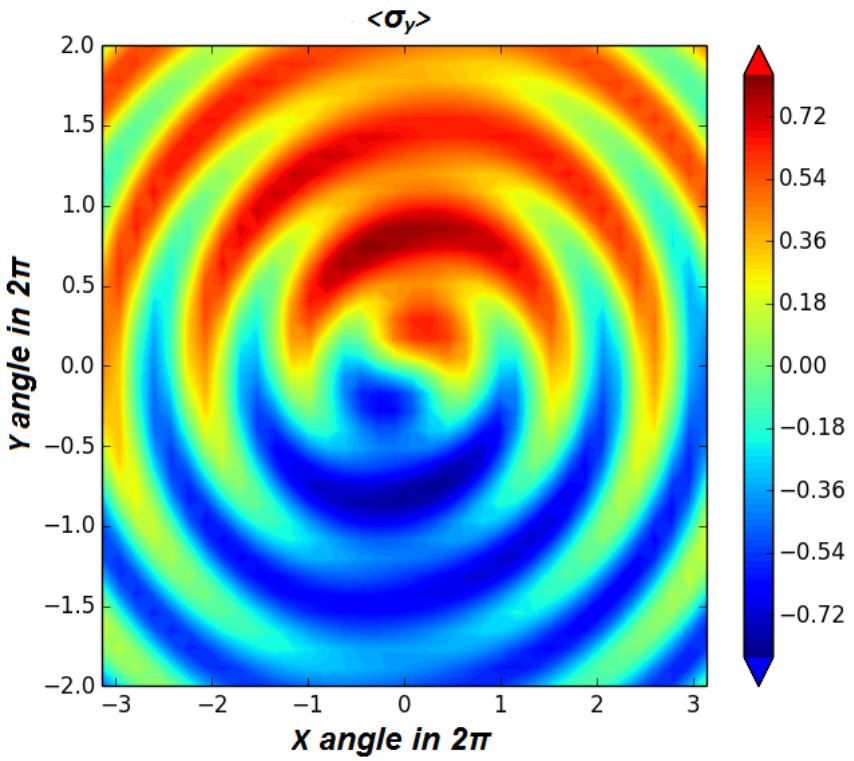
<σy>
2.0
1.5
1.0
0.5
0.0
−0.5
−1.0
−1.5
−2.0
Y angle in 2π
−3
−2
−1
0
1
2
3
X angle in 2π
0.72
0.54
0.36
0.18
0.00
−0.18
−0.36
−0.54
−0.72

(c)

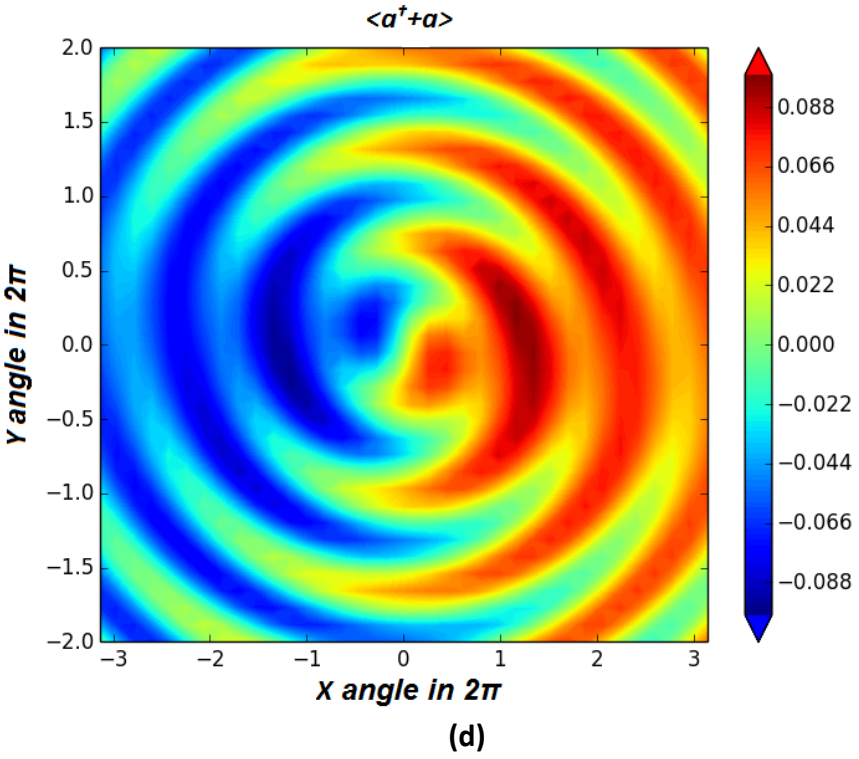
<a†+a>
2.0
1.5
1.0
0.5
0.0
−0.5
−1.0
−1.5
−2.0
Y angle in 2π
−3
−2
−1
0
1
2
3
X angle in 2π
0.088
0.066
0.044
0.022
0.000
−0.022
−0.044
−0.066
−0.088

(d)

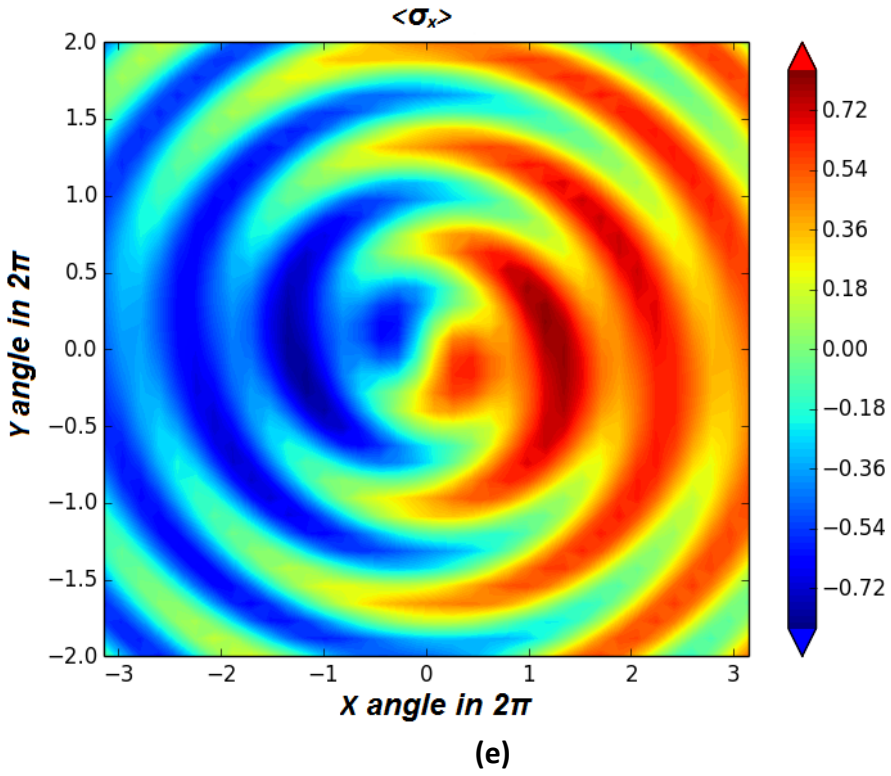

(e)

Figure 7: Single photon fluorescence tomography. **(a)**. Simulation of qubit state $\langle\sigma_z\rangle$ after rotations by pulses of arbitrary amplitude and phase. Regardless of the phase of the pulse, the qubit oscillates to a peak after a π pulse. **(b)** and **(c)**. The amplitude of the voltage in homodyne quadrature $i\langle a^{\dagger} - a\rangle$ agrees with expectations for the simulation of qubit state $\langle\sigma_y\rangle$. **(d)** and **(e)**. The amplitude of the voltage in homodyne quadrature $\langle a^{\dagger} + a\rangle$ agrees with expectations for the simulation of qubit state $\langle\sigma_x\rangle$. Oscillations around the x-axis produce a signal in $i\langle a^{\dagger} - a\rangle$ while none in $\langle a^{\dagger} + a\rangle$. This shows the ability to map an arbitrary qubit state onto a photon state, as well as the ability to characterize a qubit state through spontaneous emission.

Conclusion

A microwave source capable of generating a single photon is reported. Although there was no technique for direct detection of single photon at the time of experiment, it can be substantiated by looking at the cavity photon number states. The quadrature of the homodyne voltages of the output photons resembles the qubit states which means that there is only one photon in the system (as the qubit can interact with one photon at a time). Also from the fluorescence tomography, it is shown that an arbitrary qubit state can be mapped into a photon state thus enabling characterization of a qubit state through looking at the spontaneous emission at the output. This mapping allows the use of microwave photons as the source of true quantum information on a chip enabling on-demand single photon generation in integrated circuit for on-chip quantum optics experiment.

Reference:

1. Schuster, D. I. *et al.* Resolving photon number states in a superconducting circuit. *Nature* **445**, 515–518 (2007)
2. Oxborrow, M. & Sinclair, A. Single-photon sources. *Contemp. Phys.* **46**, 173–206 (2005)
3. Clauser, J. F. Experimental distinction between the quantum and classical field-theoretic predictions for the photoelectric effect. *Phys. Rev. D* **9**, 853–860 (1974)
4. Kimble, H. J., Dagenais, M. & Mandel, L. Photon antibunching in resonance fluorescence. *Phys. Rev. Lett.* **39**, 691–695 (1977)
5. Diedrich, F. & Walther, H.Nonclassical radiation of a single stored ion. *Phys. Rev. Lett.* **58**, 203–206 (1987)
6. Basche, T., Moerner, W. E., Orrit, M. & Talon, H. Photon antibunching in the fluorescence of a single dye molecule trapped in a solid. *Phys. Rev. Lett.* **69**, 1516–1519 (1992)
7. Brunel, C., Lounis, B., Tamarat, P. & Orrit, M. Triggered source of single photons based on controlled single molecule fluorescence. *Phys. Rev. Lett.* **83**, 2722–2725 (1999)
8. Lounis, B. & Moerner, W. E. Single photons on demand from a single molecule at room temperature.*Nature* **407**, 491–493 (2000)
9. Kurtsiefer, C., Mayer, S., Zarda, P. & Weinfurter, H. Stable solid-state source of single photons. *Phys. Rev. Lett.* **85**, 290–293 (2000)
10. Michler, P. *et al.* Quantum correlation among photons from a single quantum dot at room temperature. *Nature* **406**, 968–970 (2000)
11. Darquie, B. *et al.* Controlled single-photon emission from a single trapped two-level atom. *Science***309**, 454–456 (2005)
12. Maitre, X. *et al.* Quantum memory with a single photon in a cavity.*Phys. Rev. Lett.* **79**, 769–772 (1997)
13. Brattke, S., Varcoe, B. T. H. & Walther, H. Generation of photon number states on demand via cavity quantum electrodynamics. *Phys. Rev. Lett.* **86**, 3534–3537 (2001)
14. Moreau, E. *et al.* Single-mode solid-state single photon source based on isolated quantum dots in pillar microcavities. *Appl. Phys. Lett.* **79**, 2865–2867 (2001)
15. Santori, C., Fattal, D., Vuckovic, J., Solomon, G. S. & Yamamoto, Y.Indistinguishable photons from a single-photon device. *Nature* **419**, 594–597 (2002)
16. Pelton, M. *et al.* Efficient source of single photons: A single quantum dot in a micropost microcavity.*Phys. Rev. Lett.* **89**, 233602 (2002)
17. Kuhn, A., Hennrich, M. & Rempe, G.Deterministic single-photon source for distributed quantum networking.*Phys. Rev. Lett.* **89**, 067901 (2002)

18. McKeever, J. *et al.* Deterministic generation of single photons from one atom trapped in a cavity.*Science* **303**, 1992–1994 (2004)
19. Keller, M., Lange, B., Hayasaka, K., Lange, W. & Walther, H. Continuous generation of single photons with controlled waveform in an ion-trap cavity system. *Nature* **431**, 1075–1078 (2004)
20. A. A. Houck, D. I. Schuster, J. M. Gambetta, J. A. Schreier, B. R. Johnson, J. M. Chow, L. Frunzio, J. Majer, M. H. Devoret, S. M. Girvin & R. J. Schoelkopf. Generating single microwave photons in a circuit, *Nature* **449**, 328-331 (2007)
21. A. Blais, R.-S. Huang, A. Wallraff, S. M. Girvin, and R. J. Schoelkopf. Cavity quantum electrodynamics for superconducting electrical circuits: An architecture for quantum computation. Phys. Rev. A **69**, 062320 (2004).
22. DiVincenzo, D. P. The physical implementation of quantum computation Fortschr. *Phys.* ***48****, 771–783* (2000)
23. Purcell, E. M. Spontaneous emission probabilities at radio frequencies. *Phys. Rev.* ***69****, 681* (1946)
24. Koch, J. et al. Charge insensitive qubit design derived from the Cooper pair box. *Phys. Rev. A* ***76****, 042319* (2007)
25. Bouchiat, V., Vion, D., Joyez, P., Esteve, D. & Devoret, M. H. Quantum coherence with a single cooper pair. *Phys. Scr.* ***T76****, 165–170* (1998)
26. Wallraff, A. et al. Strong coupling of a single photon to a superconducting qubit using circuit quantum electrodynamics. *Nature* ***431****, 162–167* (2004)
27. M. Boissonneault, J. M. Gambetta and A. Blais. Dispersive regime of circuit QED: Photon-dependent qubit dephasing and relaxation rates *Phys. Rev. A* ***79****, 013819* (2009)
28. Steffen, M. et al. State tomography of capacitively shunted phase qubits with high fidelity. *Phys. Rev. Lett.* ***97****, 050502* (2006)
29. Smithey, D. T., Beck, M., Raymer, M. G. & Faridani, A. Measurement of the Wigner distribution and the density matrix of a light mode using optical homodyne tomography: application to squeezed states and the vacuum. *Phys. Rev. Lett.* ***70****, 1244–1247* (1993)
30. Leonhardt, U. Measuring the Quantum State of Light (Cambridge Univ. Press, 1997)